Structural and vibrational study of the negative thermal expansion in liquid As_2Te_3

Céline Otjacques,[1,*] Jean-Yves Raty,[1] Françoise Hippert,[2] Helmut Schober,[3] Mark Johnson,[3] René Céolin,[4] and Jean-Pierre Gaspard[1]

[1]*Condensed Matter Physics Laboratory, University of Liège, B5, B-4000 Sart-Tilman, Belgium*

[2]*LMGP-CNRS-Grenoble INP, 3 Parvis L. Néel, 38016 Grenoble-Cedex 1, France*

[3]*Institut Laue Langevin, BP 38042, BP 220, Grenoble Cedex, France*

[4]*Faculté des Sciences Pharmaceutiques et Biologiques, Université Paris Descartes, 4 av. de l'Observatoire EA4066, 75006 Paris, France*

(Received 3 March 2010; published 10 August 2010)

We present an experimental and theoretical study of liquid As_2Te_3. This alloy exhibits a negative thermal expansion (NTE) in a 250 K range above the melting temperature T_m=654 K. We evidence the changes in As_2Te_3 structure by measuring neutron-diffraction spectra at five temperatures in the NTE range and perform first principles molecular dynamics simulations at the same temperatures and densities to study the local order evolution in the liquid. Our calculated structures show an increase in the coordination numbers and a symmetrization of the first neighbors shell around atoms when the temperature rises. To confirm these results, we performed inelastic neutron scattering to obtain the vibrational density of state (VDOS) along the NTE. We see a clear change in the VDOS, consisting in a redshift of the highest frequencies with temperature. Finally, electrical conductivity evolution was obtained from the simulated structures, to compare with the semiconductor to metal transition measured experimentally.

DOI: 10.1103/PhysRevB.82.054202 PACS number(s): 65.20.−w

I. INTRODUCTION

A few covalent compounds present a negative thermal expansion (NTE) in the liquid phase, accompanied by a semiconductor to metal (SC-M) transition. Covalent elements and compounds have low coordination numbers n_c (e.g., $2 \leq n_c \leq 4$) in the crystalline and liquid phases, in comparison to the compact structures of the metals and rare gases. The low coordination number is the result of a quantum mechanical spontaneous symmetry-breaking mechanism, the Peierls distortion, leading to the octet rule in the simplest cases. The mechanism has been demonstrated to be valid for crystal structures;[1] it may still be present in liquids.[2,3] In that case, thermal effects restore in part the symmetry and increase the coordination number.

The archetypal example is Te (Refs. 4 and 5) for which the NTE (sometimes called density anomaly) occurs entirely in the undercooled liquid, in a range of about 100 K below the melting temperature T_m=723 K, with a specific heat maximum and a steep decrease in the sound velocity.[6] The thermodynamical changes are accompanied by a marked structural evolution: the coordination number n_c increases with temperature. At low temperatures (undercooled region) n_c is close to 2.4, it rises to 2.7 at the melting point and goes above 3 at high T.[7]

Another interesting system is $GeTe_6$: with the addition of a light element, Ge, the NTE takes place mostly above the melting point.[8] $GeTe_6$ has been studied in details by combining different techniques: neutron elastic and inelastic scattering, x-ray absorption spectroscopy, and *ab initio* calculations.[9–11] The structural change results in strong and anomalous variations in thermodynamic quantities among which are the density, the heat capacity, the isothermal compressibility, and the sound velocity. The analysis of the thermodynamic and neutron-scattering data suggests that the structural change undergone by the liquid mainly consists in a modification of the first neighbors shell of the Ge atoms. With increasing temperature some GeTe bonds become shorter, leading to a more compact local environment with a smaller atomic volume. The volume contraction is associated with an increase in the first neighbors coordination number around both Ge and Te by about one atom.[11] The structural evolution resulting in the NTE is accompanied by noticeable changes in the vibrational density of states spectra (redshift of the high-energy modes).[12] These evolutions can be understood as resulting from a gain of vibrational entropy that cancels out or at least weakens the Peierls distortion when the temperature increases in the NTE temperature range.[12] At low temperature, the Ge atoms are off-center in their cage of Te atoms and at higher temperatures they rattle around the center of the shrinked cage. In this picture the NTE results from competing effects (Peierls symmetry-breaking mechanism and entropic symmetry-restoring mechanism).

In order to test the generality of the structural and dynamical evolutions occurring in the NTE regime and their relation to the SC-M transition, a very interesting system is As_2Te_3. Tsuchiya measured the temperature evolution of the molar volume and found a contraction above T_m in the As_xTe_{1-x} compounds (x varying from 10 to 70).[13] For As_2Te_3, this NTE (presented in Fig. 1) extends over 250 K above T_m=654 K.[14] Electronic transport studies[15–17] show the presence of a SC-M transition in As_2Te_3 in the NTE temperature range. The dc conductivity increases from ~30 to ~1700 Ω^{-1} cm^{-1} between 673 and 973 K.[17] Many experimental and theoretical studies have been devoted to the structure of liquid As_xTe_{1-x} alloys with contradictory results. Neutron-diffraction studies on liquid As_2Te_3 were performed by Uemura[18] at 697 and 925 K and, more recently, by Maruyama *et al.*[19] in the entire NTE temperature range. In the first study, no temperature evolution was reported between 697 and 925 K. On the contrary, Maruyama *et al.* observed a strong evolution of the measured spectra between 673 and 1073 K. Endo and Ikemoto[16,17] performed extended

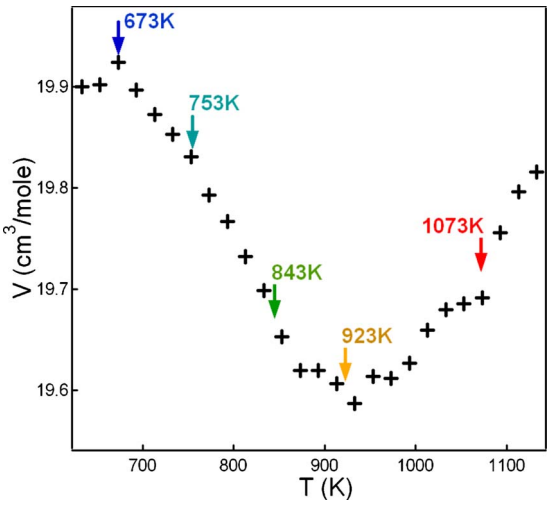

FIG. 1. (Color online) Molar volume evolution with temperature for liquid As_2Te_3 (T_m=654 K) (Ref. 13). The arrows indicate the temperatures of our experiments.

x-ray absorption fine structure (EXAFS) experiments at the As and Te *K* edges as a function of temperature for different As_xTe_{1-x} compositions in the liquid state and related the SC-M transition to structural changes. In As_2Te_3, they concluded that the atomic distances are nearly independent of temperature in a 150 K range above the melting point while coordination numbers around As and Te atoms are decreasing. They interpreted this evolution by a structural transformation from a network structure to a chain structure and associated it with the SC-M transition. They also found a non-negligible proportion of homopolar bonds. A first-principles molecular dynamic (FPMD) study of As_2Te_3 indicated structural (structure factor, partial pair correlation function) and electronic density of states (EDOS) changes with temperature.[20,21] Unlike the results of EXAFS experiments, no clear tendency of transformation from a network to a chainlike structure above the melting point was reported while an increase in the partial EDOS at the Fermi level, larger for Te than for As, was observed. It was concluded that the electronic states around Te atoms play an important role in the SC-M transition with increasing temperature. Recently, another FPMD study of liquid As_xTe_{1-x} alloys has been published,[22] in which authors compare structural, dynamical, and electronical properties for x=0.2,0.3,0.4,0.5, and 0.6 at fixed T=800 K. They also found that the total coordination number, n_c, of Te atoms slightly increases with As concentration while n_c of As atoms remains constant. Combining the structural information available from EXAFS analysis,[17] the molecular dynamics simulations results of Shimojo,[20] and neutron-diffraction spectra between 673 and 1073 K, Maruyama *et al.*[19] conclude that the SC-M transition is associated with the transformation to a denser configuration composed of shortened chain molecules. The aim of the present work is to obtain more information on the structural and dynamical evolution of As_2Te_3 in the NTE temperature range by combining neutron-diffraction and inelastic neutron-scattering experiments with *ab initio* simulations.

II. TECHNIQUES

We performed neutron-diffraction and inelastic-scattering experiments, as well as FPMD simulations on liquid As_2Te_3 at several temperatures above the melting point. The neutron-diffraction experiment was carried out on the two-axis diffractometer D4 at the Institut Laue-Langevin (Grenoble). The total scattered intensity was measured as a function of the scattering angle 2θ for an incident neutron wavelength λ=0.6970 Å. The 2θ angular range extended from 1.750° up to 138.375° with a 2θ step equal to 0.125°, which corresponds to neutron-scattering vectors $q=4\pi \sin\theta/\lambda$ in the range 0.275 to 16.853 Å^{-1}. Samples were put in quartz tubes of 8 mm internal/10 mm external diameter and sealed under vacuum. Measurements were performed at 673, 753, 843, 923, and 1073 K, i.e., in and above the NTE temperature range (see Fig. 1). The furnace is a vanadium cylindrical foil (0.1 mm thickness), its contribution to the total scattered intensity is small, temperature independent, and isotropic. The empty quartz cell signal was measured in the same furnace at 673, 923, and 1073 K. In order to obtain the scattered intensity from the samples, the contribution of the empty quartz cell was subtracted following the method of Paalman and Pings.[23] The multiple scattering was removed and Plazeck corrections[24] for inelastic scattering were carried out. We also measured a vanadium sample with a geometry identical to that of the samples, in order to get an absolute normalization of the intensity scattered by the samples. The obtained differential cross section (per atom), $d\sigma/d\Omega$, at large q coincides with the expected value ($4\pi\overline{b^2}$=4.713 barns) within a few percent, which validates the data treatment. Finally, the structure factor $S(q)$ was computed using[25]

$$\frac{d\sigma}{d\Omega} = \bar{b}^2 S(q) + \overline{b^2} - \bar{b}^2 \tag{1}$$

The neutron-scattering lengths are 6.58 fm for As and 5.80 fm for Te.[26] The neutron inelastic-scattering experiment was performed on the IN6 time-of-flight spectrometer at the ILL, using a wavelength λ=4.14 Å. Measurements were performed at 673, 803, 923, and 1073 K. We corrected the spectra by subtracting the quartz contribution and normalizing to a reference spectrum, measured on a vanadium cylinder. The data were also corrected for the energy-dependent detector efficiency and time-independent background. We then converted time-of-flight data into a dynamical structure factor $S(2\theta,\omega)$ and integrated over the whole 2θ range (10° to 115°) to obtain the vibrational density of states (VDOS) vs energy. Finally, the experimental VDOS were normalized to unity.

We performed FPMD simulations to obtain atomic trajectories on a 210 atom box (84 As and 126 Te) at the experimental liquid densities[13] (ρ=0.0302 Å^{-3} at 673 K, ρ=0.0304 Å^{-3} at 753 K, ρ=0.0306 Å^{-3} at 843 K, ρ=0.0307 Å^{-3} at 923 K, and ρ=0.0306 Å^{-3} at 1073 K). We first heated the liquid at 3000 K for 5 ps and then cooled it to desired temperatures in 20 ps. We then thermalized the liquid at the five densities and temperatures for 16 ps. We used the VASP package[27] with the PW91 exchange correlation

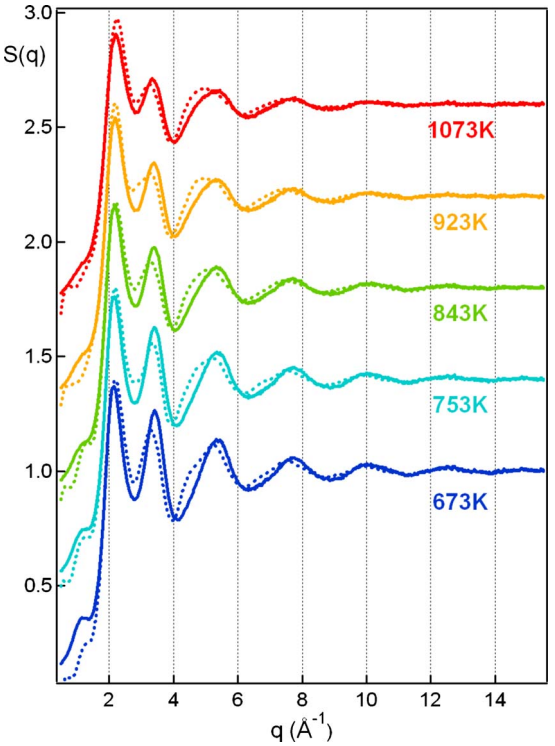

FIG. 2. (Color online) Evolution with temperature of liquid As_2Te_3 structure factor, experiment (solid lines) and FPMD results (dotted lines). The curves are vertically offset by 0.4 each for clarity.

functional,[28] ultrasoft pseudopotentials,[29] As ($4s$ and $4p$) and Te ($5s$ and $5p$) valence electrons and a planewave cutoff energy of 250 eV. Electronic calculations were performed at the Γ point only.

III. RESULTS

A. Structure

The structure factors $S(q)$ at the different measurement temperatures are presented in Fig. 2 (solid lines). They exhibit strong oscillations (up to the maximum q value of the experiment, 16 Å^{-1}) which are evolving significantly with temperature. The most striking effect is the decrease in the second and third peak heights by, respectively, 12% and 7% between the lowest temperature (673 K) and the highest one

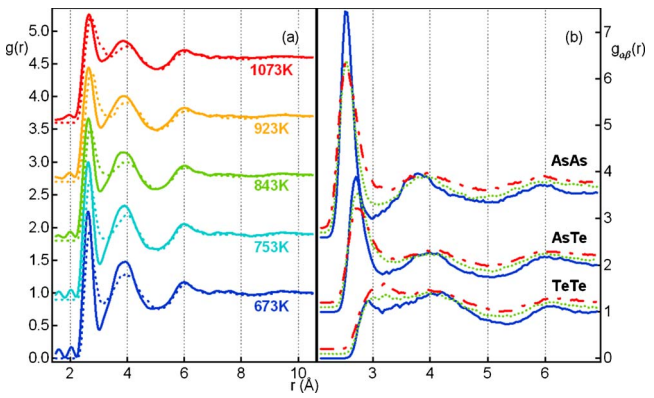

FIG. 3. (Color online) (a) Temperature evolution of the experimental pair correlation functions for As_2Te_3 (solid lines). Comparison with FPMD results (dotted lines). The curves are vertically offset by 0.8 each for clarity. (b) Partial pair correlation functions $g_{\alpha\beta}(r)$ versus temperature, from FPMD, at 673 K (solid lines, blue online), 843 K (dotted lines, green online), and 1073 K (dashed-dotted lines, red online). The curves for each kind of atomic pair are vertically offset by 1.0 each, and by 0.1 between the different temperatures.

(1073 K) while the first peak height only decreases by 5%. We also observe, at highest T, the annihilation of the prepeak located at 1.16 Å^{-1}. Between 673 and 1073 K the peak's position shifts slightly to higher q for the first (from 2.14 to 2.20 Å^{-1}) and to smaller q for the second peak (from 3.42 to 3.34 Å^{-1}). The third peak maximum position remains almost constant but a shoulder develops on its low q side. This evolution of structure factor in the NTE temperature range is similar to the results of Maruyama.[19] We performed Fourier transforms of the experimental structure factors to obtain the pair correlation functions $g(r)$, represented in Fig. 3(a) (solid lines). We can observe a strong decrease in the first and second peak heights with temperature, by 25% and 15%, respectively. Positions of the first and second maxima r_1^{exp} and r_2^{exp} and first minimum $r_{\min}^{exp}$ in $g(r)$ and coordination numbers n_c^{exp} obtained from the first peak area are reported in Table I. For each temperature, the coordination number was calculated by integrating $4\pi r^2 \rho g(r)$ from a fixed distance $r = 1.6$ Å to a cutoff distance taken equal to $r_{\min}^{exp}$. The distances r_1^{exp} and $r_{\min}^{exp}$ are slightly increasing with temperature while r_2^{exp} is slightly decreasing. The coordination number is increasing from 2.4(8) at 673 K to 2.8(6) at 1073 K.

TABLE I. Temperatures (in K), experimental liquid densities (Ref. 13), positions of the first maximum r_1^{exp} and minimum $r_{\min}^{exp}$ in experimental $g(r)$ and coordination numbers n_c^{exp}. The second decimal is indicated between parentheses. All distances are given in angstrom.

T (K)	ρ (Å^{-3})	r_1^{exp}	$r_{\min}^{exp}$	r_2^{exp}	n_c^{exp}
673	0.0302	2.62	3.02	3.92	2.4(8)
753	0.0304	2.64	3.04	3.90	2.5(3)
843	0.0306	2.64	3.08	3.84	2.6(2)
923	0.0307	2.66	3.10	3.88	2.6(9)
1073	0.0305	2.66	3.14	3.86	2.8(6)

TABLE II. Temperatures (in K), positions of the first maximum r_1^{fpmd} and minimum $r_{\min}^{fpmd}$ in total $g(r)$ from FPMD, coordination numbers n_c^{AB} (A being the central atom) from partial pair correlation functions and total coordination numbers for As and Te. The second decimal is indicated between parentheses. All distances are given in angstrom.

T (K)	r_1^{fpmd}	$r_{\min}^{fpmd}$	n_c^{AsAs}	n_c^{AsTe}	n_c^{TeAs}	n_c^{TeTe}	n_{tot}^{As}	n_{tot}^{Te}
673	2.68	3.13	1.5(1)	1.9(0)	1.2(7)	0.8(9)	3.4(1)	2.1(6)
753	2.68	3.17	1.4(9)	2.1(1)	1.4(0)	0.9(4)	3.6(0)	2.3(4)
843	2.72	3.17	1.5(6)	2.0(9)	1.3(9)	0.9(9)	3.6(5)	2.3(8)
923	2.73	3.19	1.6(2)	2.1(4)	1.4(3)	1.0(6)	3.7(6)	2.4(9)
1073	2.74	3.24	1.9(2)	2.0(9)	1.3(9)	1.3(4)	4.0(1)	2.7(3)

In Fig. 2, we also present, together with the experimental curves for comparison, the calculated $S(q)$ obtained from FPMD simulations at the same T conditions (dotted lines). The overall $S(q)$ shape is in qualitative agreement with experiment, at each temperature, up to the highest q values. More importantly, the characteristic features of the $S(q)$ thermal evolution are well reproduced by the FPMD results. The decrease in the second and third peak heights with temperature is similar for the experimental and FPMD results while the first peak height is found roughly constant in both cases. Finally, the position of the first peak of the calculated $S(q)$ agrees well with experiment, the positions of the second and third peaks being slightly shorter than the observed ones, which will lead to a distance overestimate in the calculated $g(r)$. A similar effect has been observed previously for $GeTe_6$ (Ref. 30) and is due to the generalized gradient approximation (GGA) approximation[28] which slightly overestimates the TeTe bond lengths.

In Fig. 3(a), we present (dotted lines) the total pair correlation functions obtained by the sum of partial pair correlation functions from FPMD, weighted by the neutron-scattering lengths. The agreement with experiment at the two highest temperatures is good for the whole r range while the two first peaks are slightly too low for the other temperatures. In Fig. 3(b), the calculated partial pair correlation functions $g_{\alpha\beta}(r)$ at 673, 843, and 1073 K for the AsAs, AsTe, and TeTe atomic pairs are shown. The AsAs and AsTe curves show a sharp first peak for all temperatures, slightly decreasing and broadening when T increases. The first peak of the TeTe partial pair correlation function is very small at all temperatures, it moves to higher r and broadens when heating. The positions of the first maximum r_1^{fpmd} and minimum $r_{\min}^{fpmd}$ in total $g(r)$ from FPMD, partial coordination numbers n_c^{AB} (A being the central atom) from partial pair correlation function and total coordination numbers for As and Te are reported in Table II. Coordinations numbers were calculated with a cutoff equal to $r_{\min}^{fpmd}$ for each temperature. We observe that r_1^{fpmd} and $r_{\min}^{fpmd}$ are slightly larger (by $\sim$0.08 Å in average) than in the experimental $g(r)$, as expected from the GGA approximation. As in the experiment, the coordination numbers from FPMD are increasing with temperature: the total coordination number for As is increasing from 3.4 to 4.0 between 673 and 1073 K and for Te it rises from about 2.2 to 2.7. This is surprisingly close to the n_c evolution in pure molten Te along the NTE temperature range.[7]

To obtain more insight about the evolution with temperature of the structures from FPMD simulations, we also analyzed the distribution of angles and bonds around atoms. Total angle distributions around As and Te are plotted in Figs. 4(a) and 4(b), respectively. They remain peaked around 90° and 180° when heating, around both types of atom, with a small broadening at high T. This fact indicates that the local order in liquid As_2Te_3 is very much octahedral in the temperature range studied (as most of the sites in the crystalline phase[31]).

We plotted in Fig. 5 the evolution with temperature of the six shortest distances distributions (over all the atoms in the simulation boxes) around As and Te atoms. At low temperature, the neighborhood of As and Te atoms consists of two distinct shells of "shorter" and "longer" interatomic distances. In the case of As, the first shell contains exactly three

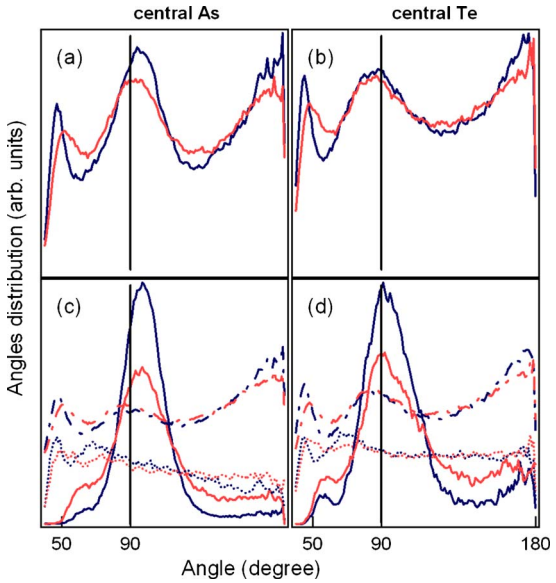

FIG. 4. (Color online) Evolution of the angle distributions with temperature. [(a) and (b)] Total angle distributions around As and Te atoms. [(c) and (d)] Partial angle distributions around As and Te. Solid lines: Distributions of angle between the three (2) first neighbors around As (Te) atoms. Dotted lines: Distributions of angle between the fourth to sixth (third to sixth) neighbors around As (Te) atoms. Dashed-dotted line: remaining angles, between the shortest and longest bonds (vertically shifted for clarity). Black lines 673 K, gray lines 1073 K (blue and red online).

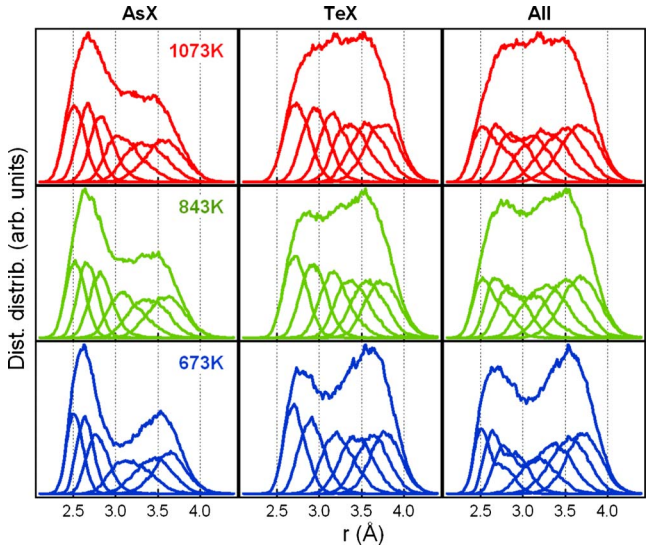

FIG. 5. (Color online) Evolution with temperature of the distance distributions around As and Te atoms, and average on both (bottom 673 K, middle 843 K, top 1073 K). The six first distance distributions are represented separately and summed.

neighbors, in the Te case it is two. When the temperature increases, the short- and long-distance distributions spread and become less distinct. Those two subshells of neighbor distributions are merging in a unique, wide, peak at high temperature in the Te case while we can still distinguish them in the As case. To see more clearly the first neighbor shell evolution, we plotted in Fig. 6 the average value of the six first distance distributions around As and Te atoms versus temperature. This figure confirms that the low-temperature

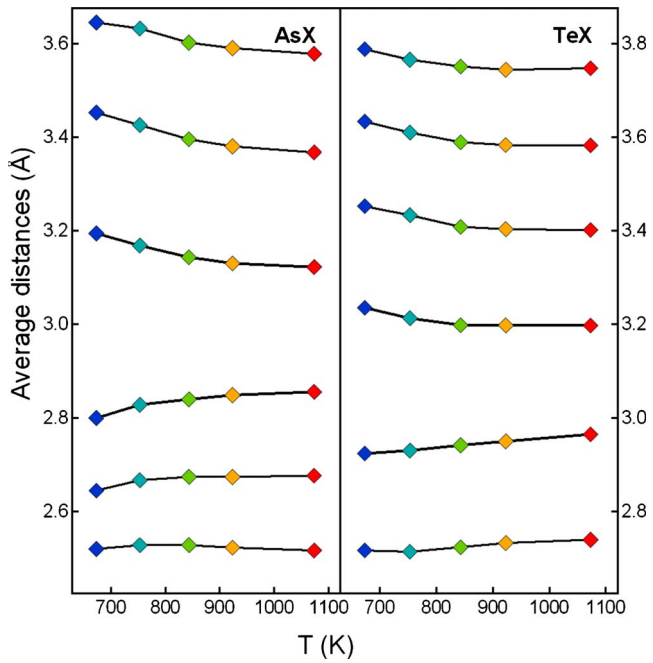

FIG. 6. (Color online) Evolution with temperature of the six average distances (from interatomic distance distributions, see Fig. 5) around As (left panel) and Te (right panel) atoms. A clear weakening of the Peierls distortion is observed, both on As and Te.

first neighbors shell, separated in three short and three long distances around As and in two short and four long distances around Te, is evolving when heating, in both cases, toward six almost regularly distributed distances. This indicates a symmetrization of the local order around both As and Te atoms. Around As, the first distance is constant when increasing temperature, the second and third distances are slightly increasing and the three largest distances shorten. Around Te, the two first distances are slightly increasing while the four largest distances decrease with T. The largest distances decrease more than the shortest ones elongate, this fact explains why the volume is shrinking when increasing temperature. These observations agree with the increase in partial coordination numbers with T, around As and Te atoms, obtained from the partial pair correlation functions (see in Table II).

In order to look for a correlation between these distance distributions and the bond angle distributions, we also calculated all the partial angle distributions a_{ij} between bonds i and j $(i,j=1,6)$ $(i \neq j)$ around As and Te atoms. In the case of As, we observed a 3+3 distance distribution at low T, so we chose to compare the sum of angle distributions a_{12}, a_{13}, and a_{23} (between the shortest bonds) to the sum of angle distributions with a_{45}, a_{46}, and a_{56} (between the longest bonds). For Te, where we observed a distance distributions of type 2+4 at low T, we compared the angle distribution a_{12} to the sum of angle distributions a_{ij} with $i,j=3,4,5,6$ $(i \neq j)$. Results are, respectively, presented in Figs. 4(c) and 4(d). One observes that the angles between the shortest bonds (solid lines) are peaked between 90° and 100° for As and around 90° for Te at all temperatures. The angle distributions are remarkably peaked for a liquid phase. We also observe a broadening of the main peak while T is rising. We do not observe any peak around 180°, which suggests that the three (As case) or two (Te case) first distances are not aligned. The angle distributions between the longest bonds (dotted lines) are very flat, indicating their softness, compared to the angles between the shortest bonds. The remaining angles (between a short and a long bond), plotted with dashed-dotted lines in Figs. 4(c) and 4(d), are peaked around 90° and 180°, indicating that the shortest and longest bonds face each other.

B. Dynamics

We performed inelastic neutron scattering (INS) to obtain the VDOS in the NTE temperature range, in order to study the changes in dynamics that could result from an evolution of local order. Results are presented in Fig. 7(a). At low energies (up to 10 meV) the VDOS follows an almost linear slope, that doesn't evolve with T. For the higher frequencies, we see a change in the VDOS shape with temperature. At low temperature, the VDOS clearly has two broad peaks, at low and high energies. When temperature increases, the high-energy peak moves toward lower frequencies, ultimately merging with the low-energy peak, and leaving only one wide peak. The largest change occurs between 673 and 923 K, thus in the NTE region. This temperature evolution in the measured VDOS shape is very well reproduced by the VDOS obtained from FPMD simulations, also shown in Fig. 7(b), although the FPMD frequencies appear to be system-

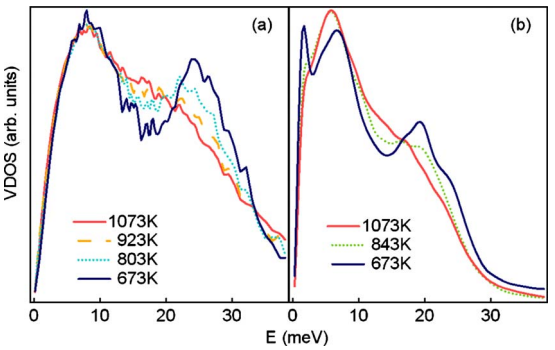

FIG. 7. (Color online) Evolution with temperature of the density of vibrational states from (a) INS experiment and from (b) FPMD trajectories.

atically underestimated by ~15%. We can also obtain partial VDOS from the FPMD trajectories, calculated on As or Te atoms separately, see Fig. 8. The high-energy part of the total spectra is mainly due to As atoms. In the discussion, we will relate the evolution in VDOS to the local order changes observed in the simulated structure.

C. Electronic properties

In the literature, liquid As_2Te_3 was mostly investigated because of its pronounced SC-M transition over a small temperature range.[15–17] We calculated the partial EDOS, for *s* states and *p* states of As and Te atoms, from the simulated structures at 673, 753, 843, 923, and 1073 K. Results are shown on Fig. 9 for selected temperatures. For both elements, the partial densities of *p* states (solid lines) exhibit a marked evolution with temperature. They present a deep minimum at the Fermi level E_F at the lowest temperature 673 K. When *T* increases from 673 to 1073 K, the *p*-state EDOS at E_F increases by ~50% for both kinds of atoms. We thus observe that *p* states from both As and Te atoms contribute almost equally to the metallization of the system.

Finally, we calculated the optical conductivities from our simulated structures by the Kubo-Greenwood formula.[32,33] Results are plotted in Fig. 10. By linear extrapolation (made between 0.5 and 1.0 eV, see Fig. 10) to zero energy we obtain the electrical conductivity evolution with temperature,

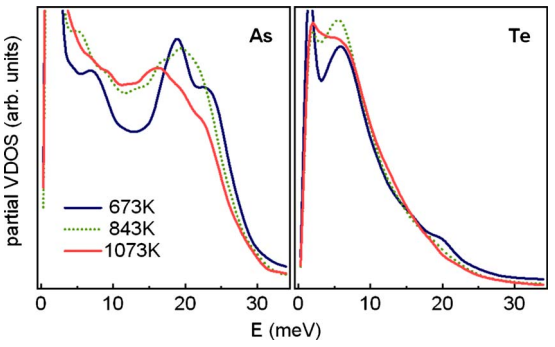

FIG. 8. (Color online) Evolution with temperature of the partial densities of vibrational states of (a) As and (b) Te on our calculated structures.

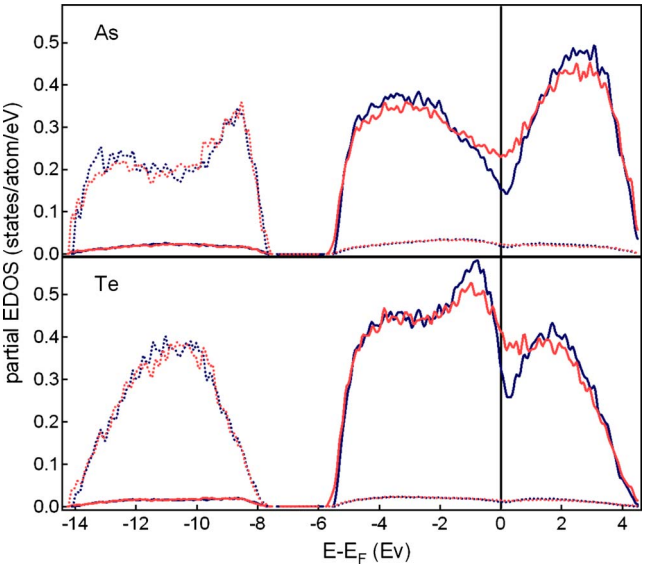

FIG. 9. (Color online) Evolution with temperature of the calculated partial densities of electronic states (in states/atom/electron volt) of As (top) and Te (bottom). Black lines 673 K, gray lines 1073 K (blue and red online). Origin of the energies is taken at the Fermi level E_F. Solid lines: *p* states. Dotted lines: *s* states.

given in Table III together with experimental results.[15,17] The latter evidence a semiconductor to metal transition with temperature in the NTE range. The measured electrical conductivity at high *T* is well reproduced by our FPMD simulations while at low *T* the calculated values are significantly higher that the experimental ones. This can be explained by the too high value of the electronic density of states at the Fermi level found in simulated structure at low temperatures, which is due to the well-known underestimation of the electronic gap of semiconductors within the DFT-GGA approximation. We nevertheless observe a steep increase in the calculated dc conductivity, which almost triples between 673 and 1073 K, giving the same trend as in the experimental observations.

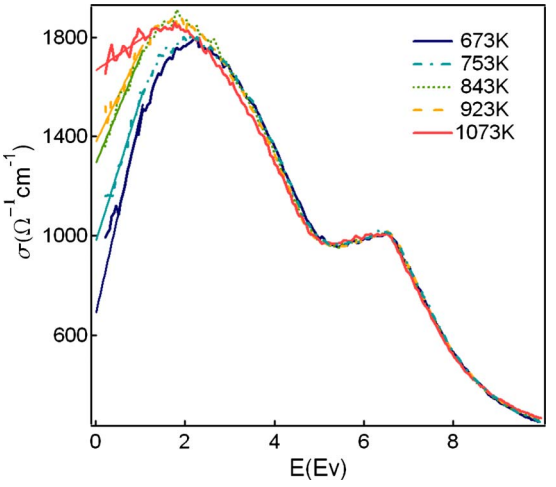

FIG. 10. (Color online) Evolution with temperature of the optical conductivities on our calculated structures and linear extrapolation to zero energy to obtain dc conductivities (thin solid lines).

TABLE III. Evolution of electrical conductivity σ (in Ω^{-1} cm^{-1}) with T (in K). Experimental results are from Refs. 15 and 17.

T	σ (Ref. 15)	T	σ (Ref. 17)	T	σ (this study)
673	28	676	30	673	684
750	12	756	192	753	981
838	531	832	658	843	1290
933	1391	901	1137	923	1376
973	1717			1073	1666

IV. DISCUSSION

From our experimental $g(r)$ and our calculated $g_{\alpha\beta}(r)$, we evidence an increase in the coordination numbers with temperature. These results are at variance with the evolution found with EXAFS experiment by Endo *et al.*,[17] despite the good agreement between first maxima of partial $g_{\alpha\beta}(r)$ from our FPMD calculations and bond lengths estimated from EXAFS analysis, reported in Table IV. In this table, the interatomic distances from other FPMD studies[21,22] are also indicated. They are in excellent agreement with the present results. In Ref. 17, the authors evidence a decrease in n_c with T, either around As or Te atoms. For As, they found that n_c, equal to 2.6 at the melting point, drops to 2 around 773 K. Around Te, they found that n_c is decreasing from around 1.5 to 1.2 in the same T range. They interpreted this decrease in partial coordination numbers by a transformation of the network structure into a chain structure composed of twofold coordinated As atoms and onefold coordinated Te atoms (*network-chain transformation*). The difference between their results and n_c evolution with T from this study may probably be attributed to the larger effective error bars on the EXAFS coordination numbers. It is actually very difficult to extract accurate coordination numbers from EXAFS experiments performed on strongly disordered, high temperature, systems, as this implies including, among others, anharmonic terms and asymmetric distance distributions. This is supported by the fact that the interatomic distances reported in[17] agree with the ones obtained in our experiment ($r_1 \sim 2.64$ Å).

Moreover the thermal evolution consisting of an increase in the number of neighbors around each type of atom in the structure (see Table II), we evidence a symmetrization of the local environment along the NTE (see Figs. 5 and 11). We show (see Fig. 6) that this effect implies the shortening of longest bonds together with the increase in shortest bonds around atoms. The volume shrinks with T because the largest distances decrease more than the shortest ones elongate. This is similar to what was observed around the Ge atoms in $GeTe_6$.[34] The increase in the shortest distances with T is correlated with the softening of vibrational modes, which explains the redshift observed in the VDOS with T (see Fig. 7). An interesting way to visualize the rate of distorsion in disordered structures, if the local order is octahedral, is to plot, with respect to distances, the probability for one central atom to have two almost aligned neighbors (which is called a three body correlation function, TBC). The result is presented in Fig. 11, for central As or Te. At low temperature, for both elements, we observe two distinct maxima in the TBC graphs, corresponding to two inequivalent distances. This means the presence of a distorsion in the local order around atoms in the structure and confirms that longer and shorter bonds are not distributed randomly between neighbors but preferentially face each other, as revealed by the partial angle distributions. When heating, the two peaks in As and Te TBC graphs are decreasing in intensity and moving toward a single peak and thus, equivalent distances. We observe that the distorsion, pronounced at low temperature, almost disappears when heating, either in the case of central As or Te. This agrees with the observations made for distance distribution evolution with T, showing the symmetrization of the first neighbors shell.

In Ref. 20, the sharp SC-M transition observed with temperature in liquid As_2Te_3 was attributed to a significant loss of chemical order. To quantify the chemical order around atoms in liquid As_2Te_3, the Warren-Cowley[35,36] short-range order parameter, $\alpha^{(i)}$, is very useful and easy to obtain from FPMD structures. It is defined by

$$\alpha^{(i)} = 1 - \frac{P_{ij}}{c_j} \quad (j \neq i = 1,2) \tag{2}$$

where c_j is the concentration of j-type atoms and P_{ij} is the probability for one i-type atom to have a j-type atom neighbor within a sphere of radius R. For a random distribution of particles $\alpha^{(i)}=0$ while a positive (negative) value indicates a

TABLE IV. First maxima of partial $g_{\alpha\beta}(r)$ from this study, compared to bond lengths obtained from EXAFS experiment (Ref. 17) and other FPMD studies (Refs. 21 and 22). The second decimal is indicated between parentheses.

	T (K)	AsAs (Å)	AsTe (Å)	TeTe (Å)
This study	673	2.5(1)	2.7(0)	2.9(4)
	843	2.5(1)	2.7(4)	3.0(0)
	1073	2.5(1)	2.7(4)	3.2(0)
Endo[a]	673	2.48	2.62	2.72
	773	2.47	2.63	2.72
Shimojo[b]	700	2.53	2.72	2.94
Zhu[c]	800	2.55	2.72	2.88

[a]Reference 17.
[b]Reference 21.
[c]Reference 22.

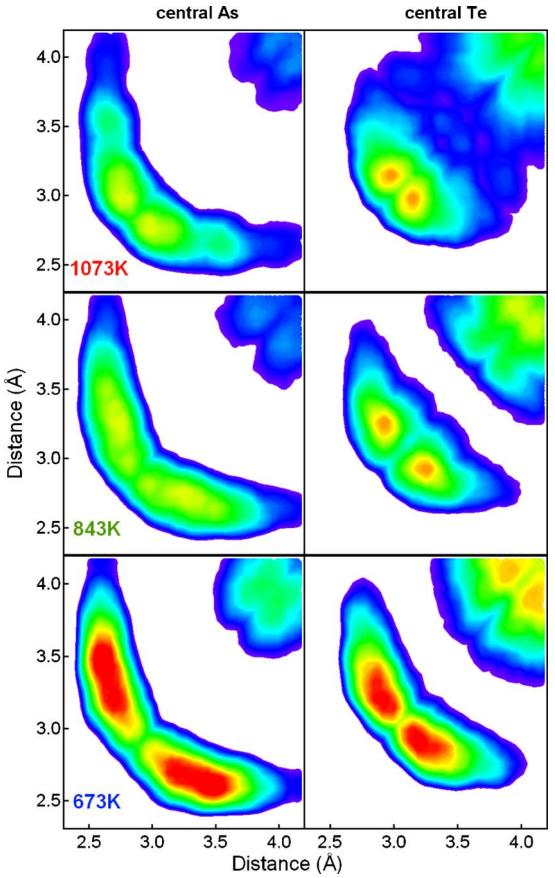

FIG. 11. (Color online) Evolution with temperature of three-body correlation functions around central As (left panel) or Te (right panel) atom. The three atoms considered are aligned with angle larger than 165°. Colors go from black (40% of the maximum, blue online) to gray (maximum, red online).

tendency to homocoordination (heterocoordination). We averaged $\alpha^{(i)}$ on all As or Te atoms in our FPMD structures at the different temperatures. We chose the radius R in two different ways: limiting the total number of neighbors to six (first neighbor shell) and to three (2) in the case of As (Te). Results are plotted in Fig. 12. For As, the short-range order parameter suggests a mostly disordered neighborhood, $\alpha^{(i)}$ being close to 0 for the different temperatures. For Te, there is a tendency to maximize the number of As among the two first neighbors. Our results for the Warren-Cowley parameter are in line with the EXAFS study made by Endo *et al.*,[17] where they demonstrated the presence of chemical disorder in liquid As_2Te_3. It is, however, interesting to note that, if little variation is observed between 673 and 923 K (the NTE

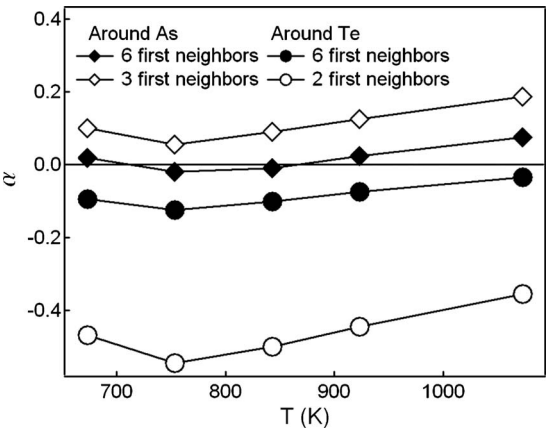

FIG. 12. Evolution with temperature of Warren-Cowley parameter $\alpha^{(i)}$ (see Eq. (2)) for As (diamonds) and Te (circles) atoms.

T range), at highest temperatures there is a clear tendency to form more AsAs and TeTe bonds inside the structure.

V. CONCLUSION

In summary, we have performed a joined experimental and theoretical study of liquid As_2Te_3. The structure of the liquid evolves from a Peierls-distorted local order to a less distorted but still octahedral, order, during the negative thermal expansion. Inelastic neutron-scattering measurements indicate that the structural changes are due to a drastic change in vibrational density of states and that the NTE is of entropic origin. This driving mechanism is similar to what was concluded previously from the study of the liquid $GeTe_6$ evolution with temperature, showing the generality of the mechanism.

In parallel, the weakening of the local Peierls distorsion is responsible for the large increase in conductivity along the SC-M transition without indication of changes in chemical order or Te chain formation.

ACKNOWLEDGMENTS

The authors thank Gabriel Cuello and Mohamed Zbiri for their help on D4 and IN6, and Christophe Bichara and Yoshimi Tsuchiya for fruitful discussions. C.O., J.Y.R. and J.P.G. acknowledge financial support from the Belgian Inter-university Attraction Pole program 3/42 and the FRS-FNRS under Grant No. FRFC 2.4505.09. J.P.G. acknowledges financial support from the Wallonie-Bruxelles International program and the FAME project. The authors wish to thank Amanuel Tewedeberhan and Stanimir Bonev.

*celine.otjacques@ulg.ac.be

[1] R. E. Peierls, *Quantum Theory of Solids* (Clarendon Press, Oxford, UK, 1955).
[2] R. Bellissent, C. Bergman, R. Ceolin, and J. P. Gaspard, Phys. Rev. Lett. **59**, 661 (1987).
[3] J.-P. Gaspard, A. Pellegatti, F. Marinelli, and C. Bichara, Philos. Mag. B **77**, 727 (1998).
[4] H. Thurn and J. Ruska, J. Non-Cryst. Solids **22**, 331 (1976).
[5] Y. Tsuchiya, J. Phys.: Condens. Matter **4**, 4335 (1992).
[6] Y. Tsuchiya, J. Phys.: Condens. Matter **3**, 3163 (1991).
[7] A. Menelle, R. Bellissent, and A. M. Frank, Europhys. Lett. **4**, 705 (1987).
[8] Y. Tsuchiya, J. Phys. Soc. Jpn. **60**, 227 (1991).
[9] R. Castanet and C. Bergman, Phys. Chem. Liq. **14**, 219 (1985).
[10] C. Bergman, C. Bichara, J.-P. Gaspard, and Y. Tsuchiya, Phys. Rev. B **67**, 104202 (2003).
[11] M.-V. Coulet, D. Testemale, J.-L. Hazemann, J.-P. Gaspard, and C. Bichara, Phys. Rev. B **72**, 174209 (2005).
[12] C. Otjacques, J.-Y. Raty, M.-V. Coulet, M. Johnson, H. Schober, C. Bichara, and J.-P. Gaspard, Phys. Rev. Lett. **103**, 245901 (2009).
[13] Y. Tsuchiya, J. Non-Cryst. Solids **250-252**, 473 (1999).
[14] J. C. Rouland, R. Ollitrault-Fichet, J. Flahaut, J. Rivet, and R. Ceolin, Thermochim. Acta **161**, 189 (1990).
[15] A. A. Oberafo, J. Phys. C **8**, 469 (1975).
[16] H. Ikemoto, H. Hoshino, T. Miyanaga, I. Yamamoto, and H. Endo, J. Non-Cryst. Solids **250-252**, 458 (1999).
[17] H. Endo, H. Hoshino, H. Ikemoto, and T. Miyanaga, J. Phys.: Condens. Matter **12**, 6077 (2000).
[18] O. Uemura, Y. Sagara, M. Tsushima, T. Kamikawa, and T. Satow, J. Non-Cryst. Solids **33**, 71 (1979).
[19] K. Maruyama, H. Hoshino, H. Ikemoto, and H. Endo, J. Phys. Soc. Jpn. **73**, 380 (2004).
[20] F. Shimojo, K. Hoshino, and Y. Zempo, J. Non-Cryst. Solids **312-314**, 349 (2002).
[21] F. Shimojo, K. Hoshino, and Y. Zempo, J. Phys.: Condens. Matter **14**, 8425 (2002).
[22] X. F. Zhu and L. F. Chen, J. Phys.: Condens. Matter **21**, 275602 (2009).
[23] H. H. Paalman and C. J. Pings, J. Appl. Phys. **33**, 2635 (1962).
[24] G. Placzek, Phys. Rev. **86**, 377 (1952).
[25] H. E. Fischer, A. C. Barnes, and Ph. S. Salmon, Rep. Prog. Phys. **69**, 233 (2006).
[26] V. F. Sears, Neutron News **3**, 29 1992.
[27] G. Kresse and J. Hafner, Phys. Rev. B **47**, 558 (1993).
[28] J. P. Perdew, J. A. Chevary, S. H. Vosko, K. A. Jackson, M. R. Pederson, D. J. Singh, and C. Fiolhais, Phys. Rev. B **46**, 6671 (1992).
[29] D. Vanderbilt, Phys. Rev. B **41**, 7892 (1990).
[30] C. Bichara, M. Johnson, and J.-Y. Raty, Phys. Rev. Lett. **95**, 267801 (2005).
[31] G. J. Carron, Acta Crystallogr. **16**, 338 (1963).
[32] R. Kubo, J. Phys. Soc. Jpn. **12**, 570 (1957).
[33] D. A. Greenwood, Proc. Phys. Soc. **71**, 585 (1958).
[34] J.-Y. Raty, J.-P. Gaspard, and C. Bichara, J. Phys.: Condens. Matter **15**, S167 (2003).
[35] B. E. Warren, *X-Ray Diffraction* (Addison-Wesley, Reading, MA, 1969).
[36] J. M. Cowley, Phys. Rev. **77**, 669 (1950).